

Tuneable Fiber Bragg Grating for Magnetic Field Sensor

Farah S. Al-Thahaby

Laser and Optoelectronics Eng. Dep.
Al-Nahrain University
galaxy.tota92@yahoo.com

Anwaar A. Al-Dergazly

Laser and Optoelectronics Eng. Dep.
Al-Nahrain University
aldergazly@gmail.com

Abstract

In this work, four fiber Bragg gratings are fabricated by infiltration different volumes of liquids (star line Glass Mechanix optical adhesive material, olive oil diluted with ethanol) into the hollow core photonic crystal fibers (HC19-1550 (Thorlab Company)). The amplitude splitting interferometric technique with a high resolution specially designed translation stage was used for the fabrication process. This stage is capable of moving the fibers in micrometer resolution steps. The fabrication was carried out using blue laser operated at wavelength of 405 nm. The infiltrated four photonic crystal fibers were exposed to the blue laser beam of 405 nm forming periodic fringes for Bragg grating generation. These fringes were generated from the interference of two splitted laser beams. All fabricated fibers have the same Bragg length of 3.8 cm and average gratings periods of 0.224 μm . The four fibers were analyzed by an optical microscope which displayed the areas that were cured using blue laser. The fabricated fibers also were tested by putting laser beam at one end of the fiber and determining the transmittance at the other fiber end by optical signal analyzer (Thorlabs-CCS200). The resulted Bragg grating fibers have 653.3 nm Bragg reflected wavelength. The results also showed that fiber with higher volume of olive oil has the highest reflection peak about 96.09647 % with the greatest FWHM (full width at a half maximum) about 0.74 nm.

In addition, three of the fabricated fibers (B, C and D) that contained olive oil were prepared for testing magnetic field sensor. The results show that all the fibers shifted to near infrared range. The results also showed that fiber with higher concentration of olive oil has the greatest magnetic wavelength shift about 653.4 nm, the highest fiber sensitivity about 0.000494623656 nm/ Gauss, the highest reflection peak about 96.91827 %, and the greatest FWHM about 0.98 nm.

Keywords: Fiber Bragg Grating, Photonic Crystal Fiber (PCF), Photosensitivity, Fiber Bragg Grating Magnetic Field Sensor, Capillary Tube, Olive Oil, Optical Adhesive.

1 Introduction

The discovery of optical fibers has developed the field of telecommunications. Over the past three decades, the developments in optical fiber

has certainly improved and reshaped fiber optic technology. In addition to applications in telecommunications, optical fibers are also used in the fields of fiber optics sensors, fiber optics lasers, and fiber optics amplifiers. Despite the enhancements in optical fiber manufacturing and progressions in the field in general, basic optical components have been a challenge to integrate with fiber optics, such as mirrors, wavelength filters, and partial reflectors. In recent times, all these have been improved with the ability to change the core refractive index in an optical fiber using optical absorption of ultraviolet (UV) light. This photosensitivity of optical fibers allows the fabrication of grating planes in the core of fibers. These gratings planes are obtained by permanently varying the refractive index in a periodic form along the core of the fiber. A periodic variation of the refractive index in the fiber core acts like a wavelength selective mirror that satisfies the Bragg condition i.e. it forms a fiber Bragg grating. The grating period and length of the grating, together with the strength of the variation of the refractive index, limited whether the grating had a high or low reflection over a wide or narrow range of wavelengths [1].

Several researches study fabrication techniques of fiber Bragg grating using Photonic crystal fiber and optical adhesive material and test it in sensing applications. Some of these researches are:

In 2006, E. Wikszak et. al. [2], had fabricated fiber Bragg gratings (FBGs) using a phase mask technique with near infrared (NIR) femtosecond laser pulses into a non-photosensitive Erbium doped fiber. A grating length of 40 mm with a grating period of 1.075 μm was realized. In 2007, Y. Lai et. al. [3], had fabricated fiber Bragg gratings with a point by point technique by a femtosecond laser. Fiber Bragg gratings with spectral quality and first-order Bragg resonances within the C-band are realized by optimizing the fabrication process. In 2008, B. Guan et. al. [4], fiber Bragg gratings were fabricated by use of two photon ultra violet excitation and characterized for temperature responses, axial strain, and hydrostatic pressure in pure-silica polarization-maintaining photonic crystal fiber. In 2009, Y. Wang et. al. [5], fiber Bragg gratings (FBGs) were fabricated in pure-silica and Ge-doped photonic crystal fibers (PCFs) with a dual-beam interference technique and a femtosecond or excimer laser. High

flexibility was observed by such a technique because it allows the fabrication of FBGs for different Bragg wavelengths. In 2010, Z. Zhang et. al. [6], had fabricated fiber Bragg grating with Bragg wavelength of 962 nm in trans-4-stilbenemethanol doped poly (methyl methacrylate) polymer optical fibers by a phase mask technique with 17% zeroth-order diffraction for the fabrication wavelength of 325 nm. In 2011, Y. Wang et. al. [7], had fabricated fiber Bragg gratings (FBGs) in two various types of small-core Ge-doped photonic crystal fibers with a UV laser. In 2012, C. M. Rollinson et. al. [8], had fabricated fiber Bragg gratings using the phase mask technique. The reflectance peaks from fiber Bragg gratings have been studied to obtain the relative importance of the grating features. In 2013, T. Elsmann et. al. [9], had fabricated fiber Bragg gratings with interferometer technique by femtosecond laser pulses of 400 nm wavelength. The interferometer technique for the fabrication process makes multiplexing practicable. In 2014, I. Bundalo et. al. [10], fiber Bragg grating (FBG) had written in Poly methyl methacrylate (PMMA) Micro structured Polymer Optical Fibers (mPOFs) using UV Phase Mask technique with writing times shorter than 10 min was demonstrated. Bragg reflection peaks were centred at 632.6 nm and have high reflection as high as 26 dB. In 2015, A. Engad et. al. [11], FBG using hollow core PCF filled with liquid mixture of olive oil and optical adhesive was designed and constructed using two-beam interferometric technique. Diode laser 405 nm used to write on fiber to make FBG with Bragg reflected wavelength (λ_B) of 806 nm.

It concluded from these studies that Bragg grating can be fabricated in a PCF. Polymers optical adhesives after exposing to laser radiation can be used to fabricate Bragg grating and the PCF can be filled with olive oil material as liquid photonic crystal.

In this research, FBGs will be fabricated in hollow core PCFs (HC19-1550 (Thorlab Company)) filled with different volumes of liquid mixture consisting from olive oil, ethanol and optical adhesive material using amplitude splitting interferometric technique, and then testing these PCFs for magnetic sensing application.

2 Fiber Bragg Gratings Principles

Gratings in a fiber are fabrication result of periodic perturbations within the fiber core. The perturbations known as grating planes are generally formed by exposing the fiber core to a UV light interference pattern, which increases the core refractive index (n_{Core}) at the points of exposure. In the simplest form, the grating planes

are perpendicular to the fiber length and have a constant grating period as shown in Figure 1 [12].

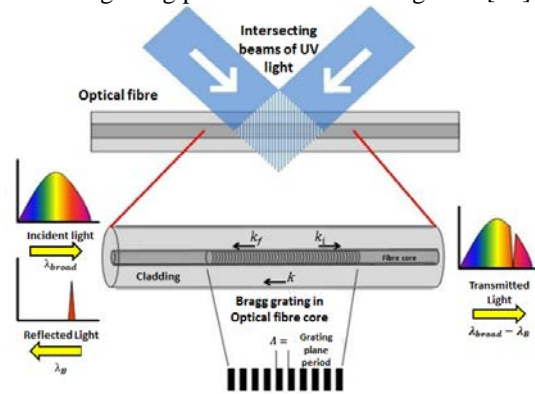


Figure 1: Illustration of uniform Bragg grating inside a fiber [13].

Phase match between the incident light that is directed along the fiber and the grating planes is required in order to reflect the light back within the core of the waveguide along counter propagating modes to meet the Bragg condition that defined by Equation (1) [12]:

$$2 \Lambda \sin\theta = m \lambda \quad (1)$$

where Λ is the grating planes period, θ is the angle between the scattering planes and the incident light, m is an integer and λ is the incident light wavelength.

The grating planes are shown in the illustration of Figure 1 as steps of index variation; however a factual illustration would look like nearer to a sinusoidal variation of refractive index along the waveguide core. The Bragg condition is met if energy and momentum is preserved. Energy preservation ($\hbar\omega_f = \hbar\omega_i$) needs that the reflected radiation frequency to be equal to the incident frequency. Momentum preservation requests that the summation of the incident wave vector (k_i) and the grating wave vector (k) is equivalent to the scattered radiation wave vector (k_f) as given by Equation (2) [12]:

$$k_i + k = k_f \quad (2)$$

When the grating wave vector (k) is perpendicular to the grating planes, then it will be equivalent to $2\pi/\Lambda$. Incident wave vector and diffracted wave vector are the same in the magnitude but reverse in the direction, so the momentum preservation condition will be as [12]:

$$\frac{4\pi n_{eff}}{\lambda_B} = \frac{2\pi}{\Lambda} \quad (3)$$

Where λ_B is the Bragg wavelength, which is the center wavelength of the reflected response and n_{eff} is the effective refractive index of the fiber core along Bragg grating length [12].

Equation (3) is simplified to give Bragg condition for the first order as follow:

$$\lambda_B = 2 n_{eff} \Lambda \quad (4)$$

The number of grating planes N is given by [14]:

$$N = \frac{l}{\Lambda} \quad (5)$$

where l is Bragg grating length.

For a uniform FBG inscribed in the optical fiber core with an index of refraction n_{eff} . The index of refraction profile $n(x)$ is given as [15]:

$$n(x) = n_{eff} + \Delta n \cos\left(\frac{2\pi x}{\Lambda}\right) \quad (6)$$

where Δn is the amplitude of the refractive index perturbation and x is the distance along the fiber longitudinal axis. The grating reflectivity with constant amplitude modulation and period can be written as [15]:

$$R(l, \lambda)_{MAX} = \frac{\Omega^2 \sinh^2(s l)}{\Delta k^2 \sinh^2(s l) + s^2 \cosh^2(s l)} \quad (7)$$

Where Ω is the coupling coefficient, $\Delta k = k - \pi/\lambda$ is the wave vector detuning, $k = 2\pi n_{eff}/\lambda$ is the propagation constant, and $s = \sqrt{\Omega^2 - \Delta k^2}$.

The coupling coefficient Ω for the sinusoidal variation of index perturbation along the fiber longitudinal axis has been found as follow [15]:

$$\Omega = \frac{\pi \Delta n \eta(V)}{\lambda} \quad (8)$$

Where $\eta(V)$ is a function of the normalized frequency V of the optical fiber that represents the fraction of the fiber mode power contained in the fiber core, $\eta(V) \approx 1 - V^{-2}$ [16]. The normalized frequency V given as follow:

$$V = \frac{2\pi r}{\lambda} \sqrt{n_{core}^2 - n_{clad}^2} = \frac{2\pi r NA}{\lambda} \quad (9)$$

where r is the core radius, n_{core} is the refractive index of the fiber core, n_{clad} is the refractive index of the fiber clad, NA is the numerical aperture.

At the Bragg wavelength, there is no wave vector detuning i.e. Δk equals zero, so the reflectivity becomes [15]:

$$R(l, \lambda)_{MAX} = \tanh^2(\Omega l) \quad (10)$$

The reflection is increased by increasing the variation of the refractive index and increasing the Bragg grating length [15].

3 Amplitude Splitting Interferometry Technique

This technique has been first used by Meltz et. al. who proved FBG fabrication results when the fiber exposed with UV interference pattern vertically on its axis. The fabrication has been done as a result of splitting the UV inscription beam into two equal intensity UV beams, and these two UV beams recombined generating UV interference pattern. Then, this interference pattern has been focussed using a cylindrical lens into the fiber core in order to increase the pattern intensity and improve the fabrication. Figure 2 shows an example of typical amplitude splitting interferometer technique. In this figure laser beam is guided to a beam splitter, to split the laser beam into two equal intensity laser beams. Both beams are reflect by the mirrors and heading for the fiber core where the two UV beams are recombined. This leads to formation of UV interference pattern in the core of the fiber. At the high intensity of this pattern, the refractive index of the fiber core is permanently varied, thus forming Bragg grating planes [17].

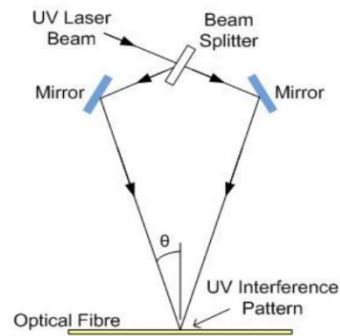


Figure 2: A typical arrangement of amplitude splitting interferometer technique [13].

The period (Λ) between the grating planes is known via the inscribing laser wavelength (λ_{UV}) and the separation angle (θ) between the two recombining UV laser beams and it is given as follow:

$$\Lambda = \frac{\lambda_{UV}}{2 \sin(\theta)} \quad (11)$$

By combining Equation (4) and Equation (11), the Bragg wavelength (λ_B) of the fabricated FBG can be written as follow:

$$\lambda_B = \frac{n_{eff} \lambda_{UV}}{\sin(\theta)} \quad (12)$$

4 Preparations of Bragg Materials

The key step used in this research is the chemical reaction of laser light effects on the photosensitive material (polymer adhesive material). The cure process of polymer adhesive depends on the intensity and the wavelength of

the laser. This reaction causes optical variation in the properties of the adhesive material as well as in the index of refraction.

The material that used in this process is star line Glass Mechanix adhesive, which is a colourless, clear liquid photo polymer adhesive. Further it has medium viscosity for bonding glass. This material is affected by the UV irradiation in a process termed "curing process", which is a converting process from liquid state into solid material state. Ultraviolet-Visible-Infrared (UV-VIS-IR) spectrophotometer is used to obtain the absorption spectrum of star line Glass Mechanix adhesive material and it's shown in Figure 3.

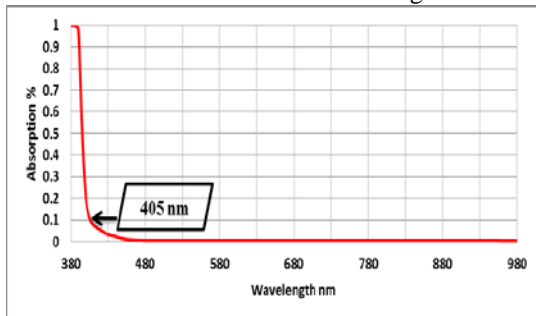


Figure 3: Illustrate the absorption of the polymer star line.

Figure 3 shows that the adhesive material star line Glass Mechanix gives maximum absorption till 385 nm wavelength. In other words, the fastest curing occurs at such maximum wavelength. Also the process of curing requires more time after 385 nm. Hence, the time of cure depends on the material absorption. Actually, there is no such a laser available at that wavelength. So, the nearest and appropriate blue laser at wavelength 405 nm is used for the fabrication. Laser diode transmittance spectrum that used in the process of curing is given in Figure 4.

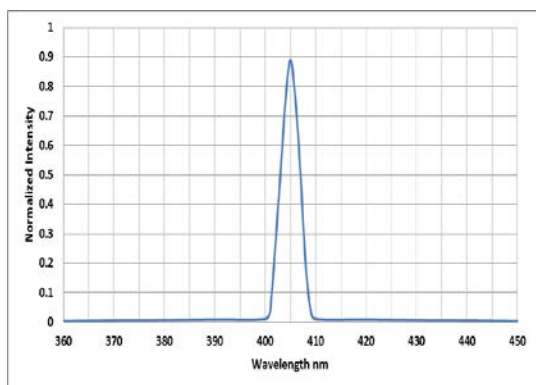


Figure 4: Laser diode spectrum of 405nm.

As given in Figure 3, the adhesive material has 10% absorption at a laser wavelength 405nm which makes it functional in this project but it needs extra time for cure. Additionally, the star line optical adhesive has a medium viscosity.

Olive Oil is an organic composite, it candidates to be used in photonics applications because it has a good nonlinear optical properties. It is used as a mixture with star line optical adhesive material. In this research, the type of olive oil is virgin. UV-VIS-IR spectrophotometer is used for measuring the optical absorption of olive oil. Figure 5 shows olive oil absorption spectrum.

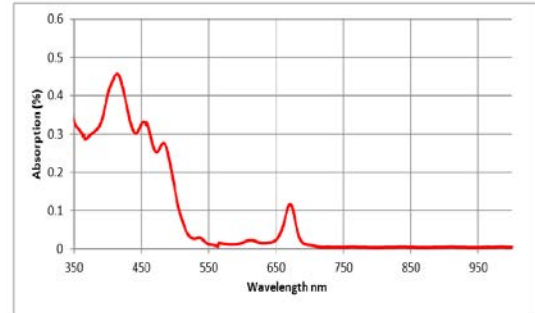


Figure 5: Olive oil absorption spectrum.

5 Fiber Infiltration

In order to fabricate Bragg gating, a photonic crystal fiber (PCF) (HC19-1550 (Thorlab Company)) hollow core type is used in this work. This PCF consists of fiber core diameter about (20±2µm), and there are air holes surrounding this fiber core, each hole has a diameter around (70±5µm) and the fiber cladding diameter of (115±3µm). Bragg grating is made by exposing the PCF (which is infiltrated with liquid mixture of adhesive material, olive oil and ethanol) to blue laser. Olive oil has higher viscosity as compared with the star line Glass Mechanix adhesive material and it must be diluted to mix with star line Glass Mechanix adhesive material. Therefore, ethanol is used with the liquid mixture because of the hydrophobic interactions between the hydrocarbon chains in olive oil and ethanol causes the one with higher viscosity to dissolve. The olive oil is diluted with ethanol before being added to the photo adhesive material. Capillary action technique is being used for infiltration the fiber in this research.

Four hollow core photonic crystal fibers (PCFs) are used.

- **PCF (A):** is infiltrated with only star line Glass Mechanix adhesive material of volume (0.12 ml/cc).
- **PCF (B):** is infiltrated with a volume (0.12 ml/cc) of liquid mixture consists of (0.06 ml/cc) star line Glass Mechanix adhesive material, (0.03 ml/cc) olive oil and (0.03 ml/cc) ethanol.
- **PCF (C):** is infiltrated with a volume (0.12 ml/cc) of liquid mixture consists of (0.04 ml/cc) star line Glass Mechanix adhesive

material, (0.04 ml/cc) olive oil and (0.04 ml/cc) ethanol.

- **PCF (D):** is infiltrated with a volume (0.12 ml/cc) of liquid mixture consists of (0.03 ml/cc) star line Glass Mechanix adhesive material, (0.06 ml/cc) olive oil and (0.03 ml/cc) ethanol.

6 Experimental Arrangement of the Fabrication Process

The experimental arrangement of the fabrication process is classified mainly into: the optical system, the linear translation stage, and the control unit as shown in Figure 6.

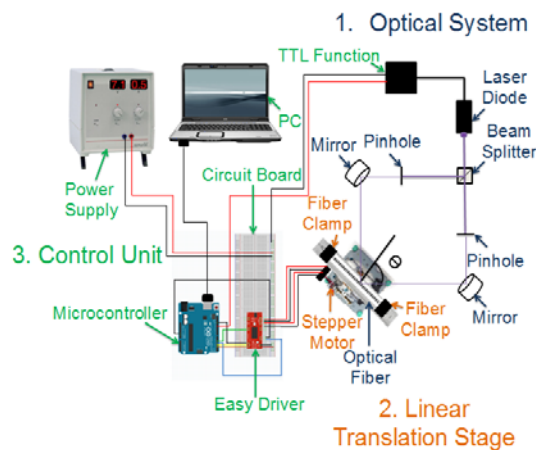


Figure 6: Experimental Arrangement diagram.

The optical system consists of an optical source, two pinholes of 1mm, two mirrors and beam splitter, as given in Figure 7. Each component has an exceptional importance for FBG fabrication.

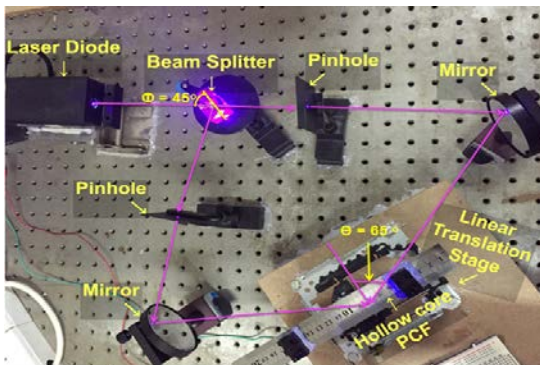


Figure 7: The path of the laser beam in the optical setup.

The optical source is a continuous wave diode laser type (SDL-405-100T) emitting at 405 nm wavelength and output power about 100 mW. It has a control unit, which is used to switch it ON/OFF. The purpose of choosing this wavelength depends on the photosensitivity of the infiltrated material inside the hollow core photonic crystal optical. In other words, this laser wavelength nearly matched the spectrum of

absorption of the star line adhesive that was infiltrated in the PCF. The profile beam of the laser diode source has elliptical shape. So, focusing this laser beam required reshaping the laser beam into circular shape. When the laser source is switched on, the laser beam is directed to a beam splitter, where it is splitted into two laser beams of the same power as shown in Figure 7. The beam splitter that is used has an incident angle about 45° in order to split the laser beam. After that these beams are directed to a dielectric mirrors to be reflected. These dielectric mirrors control the paths of the beams by adjusting these mirrors in x and in y axes. Then, these beams are recombined and creating interference fringes pattern inside the PCF core.

The linear translation stage is a stage moves linearly in z-axis only and it's consists of two fiber clamps and bipolar stepper motor as given in Figure 8.

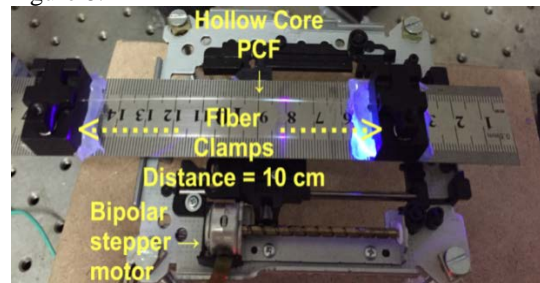


Figure 8: A translation stage that is moves linearly in z-axis.

The fiber is fixed on the stage and held by the fiber clamps. The distance separation between these clamps is 10 cm. The motor used in this stage is a bipolar Micro stepper motor, which has two phases four wires hybrid type. This motor requires dc voltage supplier about 4-6 volt. The motor has a 15 mm diameter with screw type SM15DD and 9 mm height. The rod diameter and length are 3 mm and 52.5 mm respectively. The total distance of the movable stage is 3.8 cm in one direction and the motor is moved 158 full steps to complete this distance. Motor resolution is 240 μm for each step of the stepper motor.

The Control Unit consists of motor driver board (A3967 easy driver), microcontroller board (Arduino Uno R3), power supply to supply voltage to the motor driver board and personal computer.

The Arduino is programmed by the personal computer to switch the laser diode ON and OFF by time to live function (TTL function) of the laser drive and to control a bipolar stepper motor by sending signal to the bipolar stepper motor through A3967 easy driver. These signals control the stepper motor speed, steps, and direction.

Arduino Uno R3 is programmed to do the following sequence:

- The laser is switched on by time to live function (TTL function) of the laser drive to start inscription process on the fiber for 3 minutes. To ensure that no movement or vibration occurs in place, the fiber is held firmly during this time.

- The laser is switched OFF to stop the inscription process.

- The fiber is moved by step resolution 240 μm . Then, the laser is switched ON again.

This procedure is repeated again until it covers the distance of 3.8 cm. The laser is still off for two second after each step to make sure that no additional inscription on the fiber happens through the steps movement. The total time of the inscription process of four fibers is about 32:30 hours.

7 FBG Testing Setup for Output Detection and Data Recording

It is essential to detect and record the output data of Bragg reflected response from the PCFs to makes sure if the inscription of the FBG is completed correctly and also to obtain the value of reflected Bragg wavelength.

The 651.3 nm laser source is used for testing the functionality of the PCF. The fiber clamps are used to hold the PCF. The end of the PCF is placed in front of the laser source and the other end in front of an optical signal analyzer (OSA) (Thorlabs-CCS200) for data analysis and recording. The OSA is sensitive to wavelengths ranges from 200 nm to 1000 nm. The output power of the desired wavelength before and after fabrication has been measured using OSA (Thorlabs-CCS200) . The resolution of this OSA (Thorlabs-CCS200) gives the reflection of the FBG. When the light from the laser source entered the PCF, the fabricated Bragg grating in the PCF will reflect the desired Bragg wavelength. The OSA (Thorlabs-CCS200) shows the exact amount of power that is transmitted from these Bragg grating. Therefore Bragg reflected wavelength can be obtained from the transmission spectrum.

8 Microscopic Images of the Inscription PCFs

To check PCFs visually, an optical microscope is typically used. The images of the microscope show different essential information about the PCFs properties. For example, the optical properties examination shows if the process of inscription FBG is completed successfully. Furthermore, it displays the defects that might occur during the process of inscription. The inscription results on the four PCFs are illustrated in Figures 9-12. The Bragg grating appears in the cores of the four PCFs.

Figure 9 shows PCF (A) with a 40X microscope image of fabricated FBG. It shows

that PCF (A) didn't experience any break through the process of inscription. The image that is magnified displays a nearer view of PCF core. It shows the regions that are exposed to blue light successfully. These regions illustrate the fabricated Bragg grating inside the fiber core, which are resulted from the interference of the two blue laser beams.

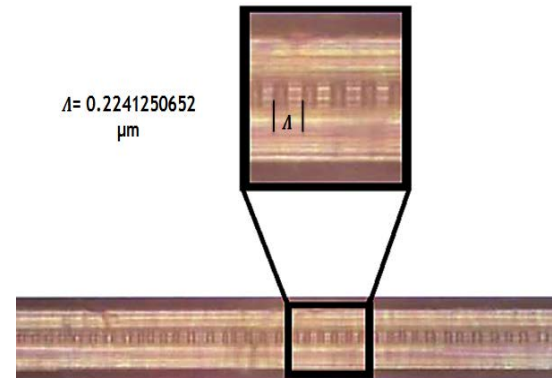


Figure 9: FBG of PCF (A) under optical microscope with average grating period 0.2241250652 μm .

Figure 10 shows PCF (B) with a 40X microscope image of fabricated FBG. It shows that PCF (B) core didn't experience any break. It displays the regions that exposed to blue light; however the image shows less clear view than PCF (A) due to the density of olive oil.

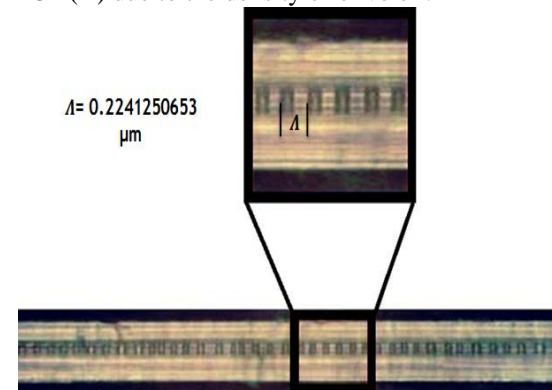


Figure 10: FBG of PCF (B) under optical microscope with average grating period 0.2241250653 μm .

Figure 11 shows PCF (C) with a 40X microscope image of fabricated FBG. It shows the regions that are cured by blue light are recognized hardly due to the higher density of olive oil than that for PCF (B).

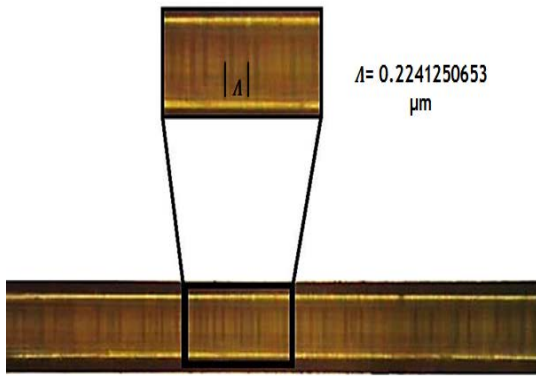


Figure 11: FBG of PCF (C) under optical microscope with average grating period 0.2241250653 μm .

Figure 12 shows PCF (D) with a 40X microscope image of fabricated FBG. It shows the regions that are cured by blue light are most hardly recognized due to the higher density of olive oil than PCF (B) and PCF (C).

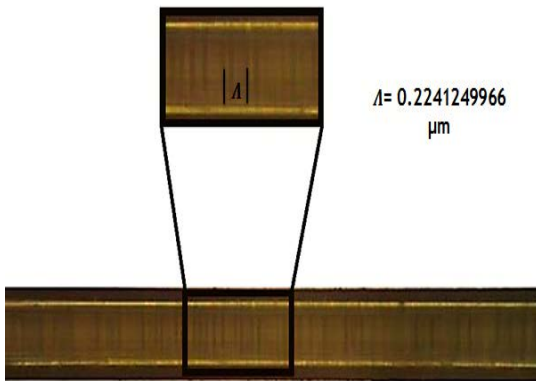


Figure (12): FBG of PCF (D) under optical microscope with average grating period 0.2241249966 μm .

PCF (A) shows clearer grating period than PCF (D) because the amount of photosensitive material is higher in PCF (A).

9 The Optical Properties

It is a process that gives the wavelength bands of the tested FBG inside PCF. This is done by directing the laser light inside the PCFs. In this research, laser at wavelength 651.3 nm is used for the testing process. The output spectrum of a PCF without any grating inscription is shown in Figure 13. It shows that, the laser directed through the PCF without any variation in the spectrum i.e. no reflection happens. This result is very important for comparison with fabricated PCFs spectrums.

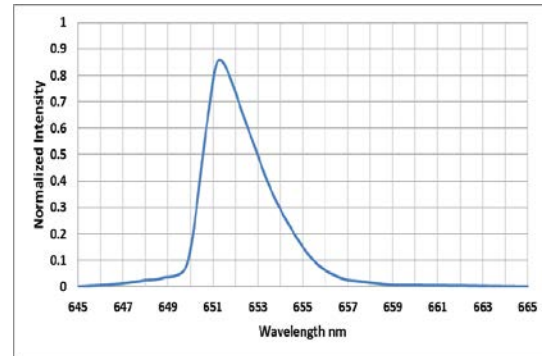


Figure 13: Transmission spectrum of 651.3 nm diode laser guided inside a hollow core PCF (HC19-1550 (Thorlab Company)) without any infiltrated material.

The fabricated FBG using star line adhesive is verified by the optical properties. The output of the laser after passing the fabricated PCF (A) is presented in Figure 14. FBG length of all PCFs is 3.8 cm. As shown in Figure 14 the output of the laser after passing PCF (A) shifts and reduce at 653.3551 nm, this wavelength (653.3551 nm) shift from the setting Bragg wavelength (651.3 nm) with experimental half angle separation $\theta = 65^\circ$ due to the setting error of the half angle separation (θ) between two interfering blue laser (405nm) correctly about 0.588% calculated from Equation (13):

$$\% \text{ Error} = \left| \frac{\text{Theoretical } \theta - \text{Experimental } \theta}{\text{Theoretical } \theta} \right| \times 100 \quad (13)$$

The theoretical half angle separation is about $\theta = 64.62^\circ$, the theoretical half angle calculated using Equation (12) by applying the values of the fabrication laser beam 405 nm, the effective refractive index of fiber (A), and the reflected Bragg wavelength of fiber (A). The effective refractive index of fiber (A) and the reflected Bragg wavelength are given in Table (1). This reduction of Bragg wavelength is because of the reflection from the periodic Bragg grating layers in the PCF core. As mentioned previously, the index of refraction and the grating period between layers determine the Bragg reflected wavelength. So, by changing the period, the peak of Bragg reflected wavelength can be blue shifted or red shifted. However, the grating period is obtained using Equation (11) using the interference created by the two blue laser beams (405 nm) that is used in FBG fabrication and using the half angle (θ) between two interfering blue laser (405nm). The FBG quality is obtained via the sharpness or the width of the reflected Bragg wavelength. Figure 14 shows a sharp drop at wavelength 653.3551 nm expressing a high precision reflection and FWHM about 0.5 nm.

The second test of FBG fabrication of PCF (B) shows a higher reflection at 653.3555438 nm with more sharpness than the previous fabricated PCF (A) and with FWHM about 0.53 nm as shown in Figure 14. The strength of reflection comes from the fact that liquid mixture is strongly cured when PCF core is irradiated by the blue laser.

The third test of FBG fabrication of PCF (C) shows a higher reflection at 653.3565367 nm with more sharpness than the previous two fabricated PCFs (A and B) with FWHM about 0.7 nm as shown in Figure 14. The strength of reflection comes from the fact that this mixture is much strongly cured when PCF core is irradiated by the blue laser.

The fourth test of FBG fabrication of PCF (D) shows the highest reflection at 653.3582 nm with much more sharpness than the previous fabricated PCFs (A, B, and C) with FWHM about 0.74 nm as shown in Figure 14. The strength of reflection comes from the fact that this mixture is much more strongly cured when PCF core is exposed to the laser irradiation.

The comparisons between the four fabricated PCFs spectrums show that, using the PCF (D) gives an enhanced output spectrum, generating a sharpest output with greater reflection depth and widest FWHM. Hence, decreasing Bragg grating length is necessary for the process of inscription because this will decrease the cost. In other words to get the same reflectivity results for PCFs (A, B, and C), Bragg grating length of these three PCFs must be doubled or tripled and this will effect on the cost and the time of the inscription process, because the reflectivity increases by the increasing of Bragg grating length [15]. The four PCFs output spectrums are presented in Figure 14.

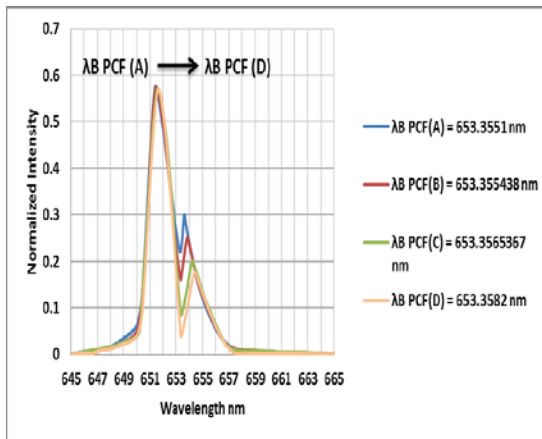


Figure 14: The transmission spectrums of the fabricated FBGs in four PCFs.

Table (1) gives the numerical examination of the four PCFs spectrums. The variation of Bragg reflected wavelength $\Delta\lambda$ of the four PCFs was measured by subtracting the setting Bragg wavelength (651.3 nm) from λ_B of the four PCFs.

Bragg reflected wavelength λ_B of the four PCFs was measured using OSA and given in Table (1).

The effective refractive indices of the four PCFs were calculated using Equation (4) by knowing the Bragg reflected wavelength of the four PCFs from Table (1) and the grating periods of the four PCFs (which were measured from the microscope images using (Image J) program).

However, the variation of the indices of refraction Δn is changes with little quantity for the four PCFs and it was calculated by subtracting the effective refractive index of the setting Bragg wavelength 651.3 nm (which is equal to 1.457560497 and its calculated using Equation (12) by knowing the inscription wavelength 405 nm and the half angle separation 65°) from the effective refractive indices of the four PCFs given in Table (1).

The reflectivity of the four PCFs were measured from the transmission spectrums.

The liquid mixtures (PCFs (B, C, and D)) full width at half maximum (FWHM) are more than that of the PCF (A), FWHM of the four PCFs were measured from the transmission spectrums.

Table 1: The variations between the four PCFs.

Injected material	λ_B (nm)	$\Delta n \times 10^{-6}$	n_{eff}	$\Delta\lambda$ (nm)	Reflctivity %	FWHM (nm)
PCF (A)	653.3551	7.623	1.45756812	2.0178723	76.20	0.5
PCF (B)	653.3555438	8.613	1.45756911	2.0183161	82.87532	0.53
PCF (C)	653.3565367	10.828	1.4575713250	2.019309	91.49684	0.7
PCF (D)	653.3582	14.985	1.457575482	2.0209723	96.09647	0.74

It can be noticed from the previous results that PCF (D) has the highest reflection due the concentration of olive oil, because olive oil has absorbance peak appears at the reflected Bragg wavelength and emission peak when the material

excited at the same wavelength as shown in Figure 15 [18].

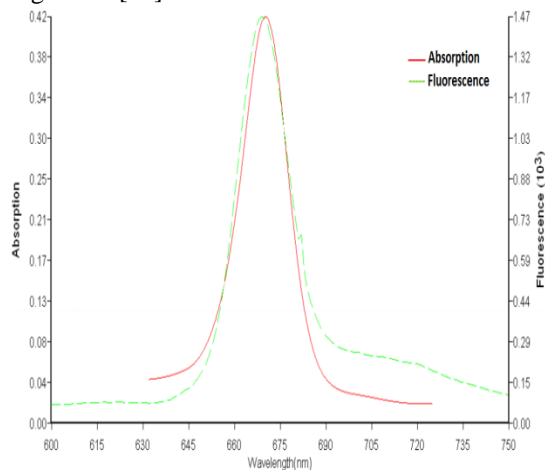


Figure 15: The absorbance peak of olive oil appears at wavelength 669 nm and its emission peak when the material excited at that wavelength [18].

10 Experimental Setup of Magnetic Field Sensor :

The experimental setup of the magnetic field sensor as shown in Figure 16 used to test the magnetic field sensing on fiber Bragg grating by measuring Bragg reflected wavelength shift of three types of PCFs (B, C and D).

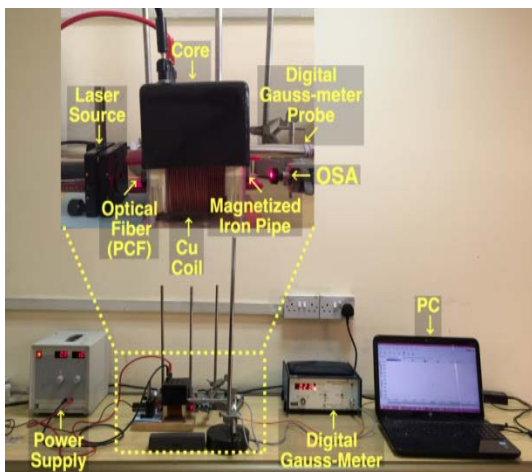


Figure 16: The experimental setup of magnetic field sensor.

The experimental setup, which is shown in Figure 16, consists of:

1. Laser diode source, which has wavelength around 650 nm, pumps the light inside hollow core photonic crystal fiber (HC19-1550 (Thorlab Company)) .
2. Magnetic field source:
 - A. Power supply is used to provide the electrical current needed to generate the magnetic field by changing the electrical current values from 1A to 5 A at a certain voltages.
 - B. Core with a copper coil is connected to the power supply in order to provide the electrical

current needed to generate the the magnetic field inside an iron pipe of 10 cm length.

3. Hollow core photonic crystal fiber (HC19-1550 (Thorlab Company)) held inside the magnetized iron pipe is used to test magnetic sensitivity. Bragg reflected wavelength shift is measured in the presence of the magnetic field.
4. Digital Gauss-meter (DGM-202) with an axial probe.
5. Optical spectrum analyzer (OSA) (Thorlabs-CCS200) is used for data analysis and recording.
6. PC is used to display the data analysis and recording.

First, the power supply was set at voltage value where the current reaches 1A. Then the magnetic flux density value is measured with the digital Gauss-meter axial probe. After the light had coming out from PCF (B), it was visualized by OSA to measure Bragg reflected wavelength. The previous procedures of measuring the magnetic flux density and Bragg reflected wavelength shift for current values of (2, 3, 4 and 5 A) were repeated for PCF (B). The two others PCFs (C) and (D) follow the same procedure of the PCF (B).

11 The Optical Properties Results of Bragg Reflected Wavelength Shifts:

The experimental setup of magnetic field sensor was used to measure the optical spectrums of Bragg reflected wavelength shifts. These spectrums are obtained by changing the magnetic flux density within a range of (0-93 Gauss). Both the magnetic flux density and Bragg reflected wavelength shifts are measured using axial probe and OSA, respectively.

11.1 PCF (B)

Figure 17 shows the spectrums of different Bragg reflected wavelength shifts of PCF (B). Table (2) gives more information about the numerical examination of these spectrums.

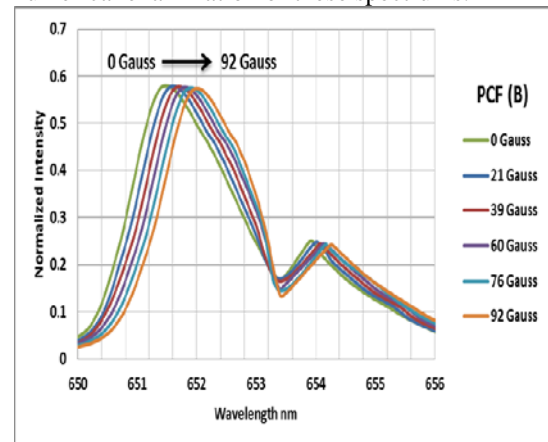


Figure 17: The spectrums of different Bragg reflected wavelength shifts of PCF (B) .

Table (2): The numerical examination of PCF (B).

Electrical Current (A)	Magnetic Flux density (Gauss)	λ_B (nm)	Reflectivity %	FWHM (nm)
0	0	653.3555438	82.87532	0.53
1	21	653.3617	82.95165	0.5302
2	39	653.3714	83.07888	0.5305
3	60	653.3808	83.20611	0.5308
4	76	653.3894	83.50120	0.5312
5	92	653.3975	83.62341	0.5315

11.2 PCF (C)

Figure 18 shows the spectrums of different Bragg reflected wavelength shifts of PCF (C). More details, which are measured from Figure 18, are written in Table (3).

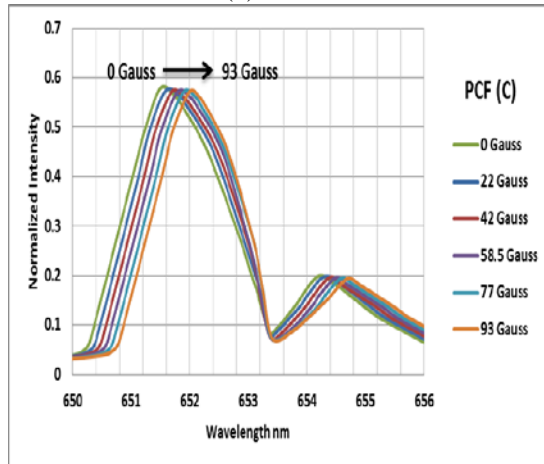


Figure 18: The spectrums of different Bragg reflected wavelength shifts of PCF (C) .

Table (3): The numerical examination of PCF (C).

Electrical Current (A)	Magnetic Flux density (Gauss)	λ_B (nm)	Reflectivity %	FWHM (nm)
0	0	653.3565367	91.49684	0.7
1	22	653.3625	92.13524	0.8
2	42	653.3723	92.4878	0.85
3	58.5	653.3813	92.54204	0.88
4	77	653.3899	92.58724	0.92
5	93	653.3980	92.67764	0.97

11.3 PCF (D)

Figure 19 shows the spectrums of different Bragg reflected wavelength shifts of PCF (D). Table (4) explains more information that measured from these spectrums.

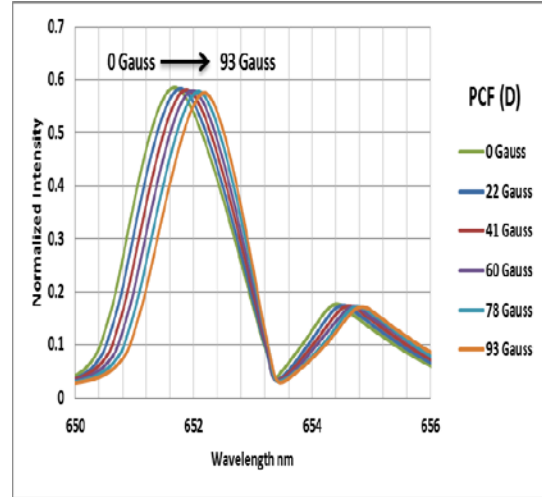


Figure 19: The spectrums of different Bragg reflected wavelength shift of PCF (D).

Table (4): The numerical examination of PCF (D).

Electrical Current (A)	Magnetic Flux density (Gauss)	λ_B (nm)	Reflectivity %	FWHM (nm)
0	0	653.3582	96.09647	0.74
1	22	653.3686	96.50737	0.83
2	41	653.3750	96.61009	0.86
3	60	653.3840	96.71282	0.89
4	78	653.3911	96.81554	0.94
5	93	653.4	96.91827	0.98

The relation between the magnetic flux density and Bragg reflected wavelength shifts of three PCFs (B, C, and D) are plotted in Figure 20.

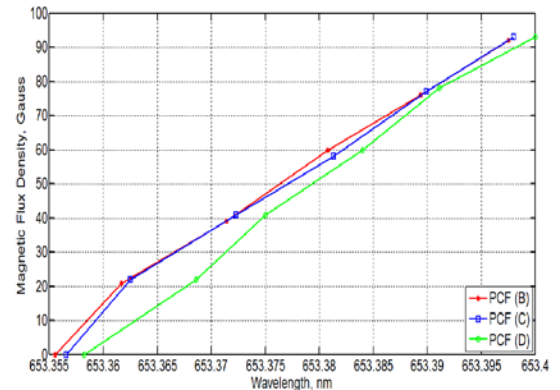


Figure 20: Comparison between the magnetic flux density versus Bragg reflected wavelength shifts of three PCFs (B, C, and D).

The curves in Figure 20 above show that increasing in the magnetic flux density due to the linear relation with the electrical current leads to shifting the Bragg reflected wavelengths of the three PCFs to NIR range. This is happened because olive oil has a positive Verdet constant equals to (98.6808 rad/T. m) at the Bragg reflected wavelength [19].

As seen in Figure 20, the PCF (D) has the greatest average wavelength shift per magnetic flux density sensitivity (0.000494623656 nm/Gauss) than the PCFs (B and C) which are of average wavelength shift per magnetic flux density sensitivity (0.0004560456522 nm/Gauss) and (0.000482518919 nm/Gauss); respectively. This is happened due to the different concentrations of olive oil that used as photonic crystal material in the three PCFs. Therefore a PCF with larger concentration of olive oil has the greatest sensitivity.

12 Conclusions

The important facts, which are concluded from the experimental results of this work, can be given as follow:

1. The fabrication setup is able to fabricate Bragg grating in four PCFs filled with liquids of different concentrations consisting of olive oil, star line Glass Mechanix adhesive material and ethanol using amplitude interferometric technique with Bragg reflected wavelength (λ_B) of 653.3 nm and reflectivity ranges equal to (PCF(A)=76.20 %, PCF (B) =82.87532 %, PCF (C) =91.49684 %, PCF (D) = 96.09647 %).

2. Increasing the concentration of olive oil in the liquid mixture that infiltrated inside PCFs gives a remarkable shift in the fabricated Bragg reflected wavelength due to the nonlinear properties of olive oil [18].

3. The results show that increasing the concentration of olive oil in the liquid mixture that infiltrated inside PCFs giving the highest reflectivity because olive oil has an absorption and an emission peaks when it excited at the fabricated Bragg reflected wavelength (653.3 nm) [18].

4. The Bragg fibers that fabricated can be used as magnetic sensor.

5. The results of applying FBG in magnetic field sensing show that increasing the magnetic flux density will increase the shift of Bragg reflected wavelength. As well as increasing olive oil concentration in the liquid mixture that infiltrated inside PCFs giving a remarkable wavelength shift to NIR range because olive oil at this fabricated Bragg wavelength has positive Verdet constant equals to (98.6808 rad/T. m) [19], so PCF (D) is more sensitive compared to other PCFs (B and C).

6. Increasing olive oil concentration in the liquid mixture that infiltrated inside PCF (D) gives a noticeable wavelength shift sensitivity about (0.000494623656 nm/ Gauss).

7. The sensitivity of the three PCFs (B, C, and D) is higher compared to the sensitivity of a PCF without Bragg grating and filled with only olive oil about (0.0003509 rad/Gauss) at 650 nm

wavelength by dividing the rotation angle per the magnetic flux density [19].

8. The FWHM is increased linearly with the increasing of Bragg reflected wavelength for all PCFs due to their direct proportional relation [14].

9. The shift in wavelength due to the magnetic field is a linear shift.

10. The reflectivity increases linearly with the increasing in magnetic flux density.

References

- [1] A. Othonos, "Review of Scientific Instruments: Fiber Bragg gratings", American Institute of Physics, Vol. 68, No.12, 1997, PP. 4309-4341.
- [2] E. Wikszak, J. Thomas, J. Burghoff, B. Ortaç, J. Limpert, S. Nolte, "Erbium Fiber Laser Based on Intracore Femtosecond-Written Fiber Bragg Grating", Optics Letters, Vol. 31, No.16, 2006, PP. 2390-2392.
- [3] Y. Lai, K. Zhou, K. Sugden, and I. Bennion, "Point-by-point Inscription of First Order Fiber Bragg Grating for C-Band Applications", Optics Express, Vol. 15, No. 26, 2007.
- [4] B. Guan, D. Chen, Y. Zhang, H. Wang, H. Tam, "Bragg Gratings in Pure-Silica Polarization Maintaining Photonic Crystal Fiber", IEEE photonics technology letters, Vol. 20, No. 23, 2008.
- [5] Y. Wang, H. Bartelt, M. Becker, S. Brueckner, J. Bergmann, J. Kobelke, M. Rothhardt, "Fiber Bragg grating Inscription in Pure-Silica and Ge-Doped Photonic Crystal Fibers", Applied Optics, Vol. 48, No. 1, 2009.
- [6] Z. Zhang, C. Zhang, X. Tao, G. Wang, and G. Peng, "Inscription of Polymer Optical Fiber Bragg Grating at 962 nm and Its Potential in Strain Sensing", IEEE Photonics Technology Letters, Vol. 22, No.21, 2010.
- [7] Y. Wang, H. Bartelt, W. Ecke, R. Willsch, J. Kobelke, "UV-Laser-Inscribed Fiber Bragg Gratings in Photonic Crystal Fibers and Sensing Applications", Proc. SPIE 8201 International Conference on Optical Instruments and Technology: Optoelectronic Measurement Technology and Systems, Vol. 8201, 2011.
- [8] C. M. Rollinson, S. A.Wade, B. P. Kouskousis, D. J. Kitcher, G.W. Baxter, and S. F. Collins, "Variations of the Growth of Harmonic Reflections in Fiber Bragg Gratings Fabricated Using Phase Masks", J. Opt. Soc. Am. A, Vol. 29, No. 7, 2012.
- [9] T. Elsmann, T. Habisreuther, A. Graf, M. Rothhardt, and H. Bartelt, "Inscription of First-Order Sapphire Bragg Gratings Using 400 nm Femtosecond Laser Radiation", Optics Express, Vol. 21, No. 4, 2013.
- [10] I. Bundalo, K. Nielsen, C. Markos, O. Bang, "Bragg Grating Writing in PMMA

Microstructured Polymer Optical Fibers in Less Than 7 Minutes ", Optics Express, Vol. 22, No. 5, 2014.

[11] A. Engad, H. M. Ahmed and A. A. Al-Dergazly, " Photonic Crystal Fiber Bragg grating Using Olive Oil as Liquid Photonic Crystal and Adhesive Material for Construction", IJSET -International Journal of Innovative Science, Engineering & Technology, Vol. 2, No. 3, 2015.

[12] A. Othonos and K. Kalli, "Fiber Bragg Gratings: Fundamentals and Applications in Telecommunications and Sensing", Norwood, MA: Artech House Publishers, 1999.

[13] I. P. Johnson, "Grating Devices in Polymer Optical Fibre", Aston University, August 2011.

[14] R. C. S. B. Allil, M. M. Werneck, B. A. Ribeiro, F. V. B. de Nazaré, " A Guide to Fiber Bragg Grating Sensors: Current Trends in Short- and Long-period Fiber Gratings", Laborde C. C. (Ed.), InTech, 2013.

[15] D. K. W. Lam and B. K. Garside, "Characterization of single-mode Optical

fiber filters", Appl. Opt., Vol. 20, No.3, 1981, PP. 440-445.

[16] D. Marcuse, "Loss Analysis of Single-Mode Fiber Splices", the Bell System Technical Journal, Vol. 56, No. 5, 1977, PP. 703-718.

[17] G. Meltz, W. W. Morey and W. H. Glenn, "Formation of Bragg gratings in optical fibers by a transverse holographic method", Optics Letters, Vol. 14, No. 15, 1989, PP. 823-825.

[18] O. N. Mohammed and A. A. AL – Dergazly, "Measurement the Fluorescence Parameters of the Olive Oil and comparing it with Some Laser Dye Materials", Baghdad university, Journal of Engineering, Vol. 16, No.1, 2010, PP. 4527-4534.

[19] A. Shakir , R.D. AL-Mudhafa, and A. A. AL–Dergazly, "Verdet Constant Measurement of Olive Oil for Magnetic Field Sensor ", International Journal of Advances in Electrical & Electronics Engineering, Vol. 2, No. 2, 2013, PP. 362-368.

ألياف براك المحززة القابلة للضبط لتحسس المجال المغناطيسي

أنوار عبد الستار الدرگزلي
قسم هندسة الليزر والالكترونيات البصرية
جامعة النهريين

فرح سالم الذهبي
قسم هندسة الليزر والالكترونيات البصرية
جامعة النهريين

الخلاصة

تم في هذا البحث تصنيع أربعة ألياف براك المحززة وذلك بحقنها بمختلف الاحجام من السوائل (المادة الصمغية البصرية star line Glass Mechanix، زيت الزيتون مذاب مع الايثانول) بداخل الجوف لتلك الالياف البلورية الفوتونية. تقنية تداخل تقسيم السعة مع منصة انتقالية مصممة خصيصاً وبدقة عالية استخدمت في عملية التصنيع. التصنيع تم باستخدام ليزر أزرق يعمل عند الطول الموجي 405 نانو متر. الألياف البلورية الفوتونية الأربعة المحقونة تم تعريضها لأشعة الليزر الأزرق ذو الطول الموجي 405 نانو متر مكونة اهداباً متكررة بشكل دوري لتوليد حزوز براك. هذه الأهداب تولدت من تداخل شعاعي الليزر الأزرق المنقسمين ذوي الطول الموجي 405 نانو متر. طول البراك المصنع للألياف يساوي 3.8 سم و معدل فترة الحزوز تساوي 0,224 مايكرو متر. الألياف الأربعة تم تحليلها بواسطة المجهر البصري والذي أظهر المناطق التي تمت معالجتها بأستعمال الليزر الأزرق. الألياف المصنعة تم فحصها أيضاً عن طريق وضع ليزر عند احدى نهايتي الليف وقياس النفاذية عند النهاية الأخرى بأستخدام محلل الأشارة البصرية (Thorlabs-CCS200). ألياف براك المحززة صنعت عند الطول الموجي لبراك 653.3 نانو متر. وكذلك أظهرت النتائج أن الليف ذي الحجم الأعلى من زيت الزيتون يمتلك أعلى قمة أنعكاسية حوالي 96,09647% نانو متر و أكبر عرض كامل عند الحد الأعلى للمنتصف حوالي 0,74 نانو متر.

بالإضافة، ثلاثة من الألياف المصنعة (PCF (B, C, and D) والتي تحتوي على زيت الزيتون تم فحصها كمتحسس للمجال المغناطيسي. أظهرت النتائج بأن كل الألياف تتحرك نحو الأشعة تحت الحمراء القريبة. وكذلك أظهرت النتائج بأن الليف ذي الحجم الأعلى من زيت الزيتون يمتلك أعلى تحسس مغناطيسي في الطول الموجي حوالي 653.4 نانو متر، أعلى الألياف حساسية بمقدار 0.000494623656 نانو متر اجاوس، أعلى قمة أنعكاسية حوالي 96,91827% نانو متر و أكبر عرض كامل عند الحد الأعلى للمنتصف حوالي 0,98 نانو متر.